

Computational Modelling of Deconstructable Composite Steel-Concrete Beams

M.A. Bradford and Y.-L. Pi
Centre for Infrastructure Engineering and Safety
School of Civil and Environmental Engineering
The University of New South Wales, Sydney, Australia

Abstract

This paper addresses the computational modelling of composite steel-concrete beams that are assembled for “deconstructability”, insofar as they can be disassembled at the end of the life of a building and hence they lessen the carbon footprint of the structure in a whole life-cycle assessment. Establishing design paradigms for such elements is difficult without recourse to numerical procedures, and so the paper focuses on a computational technique for composite beams constructed by bolting the concrete slab to the steel joist with high-strength bolts that act as shear connectors. An elastic-plastic geometrically non-linear computational formulation is established, that can handle the relative interface slip with an empirical representation in algebraic form. The finite element (FE) technique is validated with tests, that demonstrate its efficacy and scope.

Keywords: deconstructability, composite beams, high-strength bolts, non-linearity, shear connection.

1 Introduction

Composite steel-concrete beams are common in engineering structures, taking advantage of the favourable compressive strength of the concrete slab and the favourable tensile strength of the steel girder in a symbiotic fashion. Mechanical shear connection between these two components is essential to realise the increased strength and stiffness of composite beams above those of the slab and steel girder alone. Because of this, headed mechanical stud shear connectors have found close to universal acceptance in contemporary buildings and bridges in providing robust shear connection between the slab and girder, being installed very economically by rapid automatic welding procedures.

Paradigms related to sustainability and full life-cycle assessment in building construction and usage are being introduced in many nations in response to climate

change, and unfortunately composite beams with headed stud connectors are not able to be decommissioned easily and efficiently during deconstruction or building modification. One means of circumventing this drawback is to use high strength bolts to provide the shear connection in lieu of headed connectors welded to the steel girder's top flange, which can be unbolted to deconstruct the building or to alter part of it structurally. Surprisingly, this form of shear connection has received little attention in published comprehensive research outcomes, despite its attractiveness for deconstruction as well as structural retrofit.

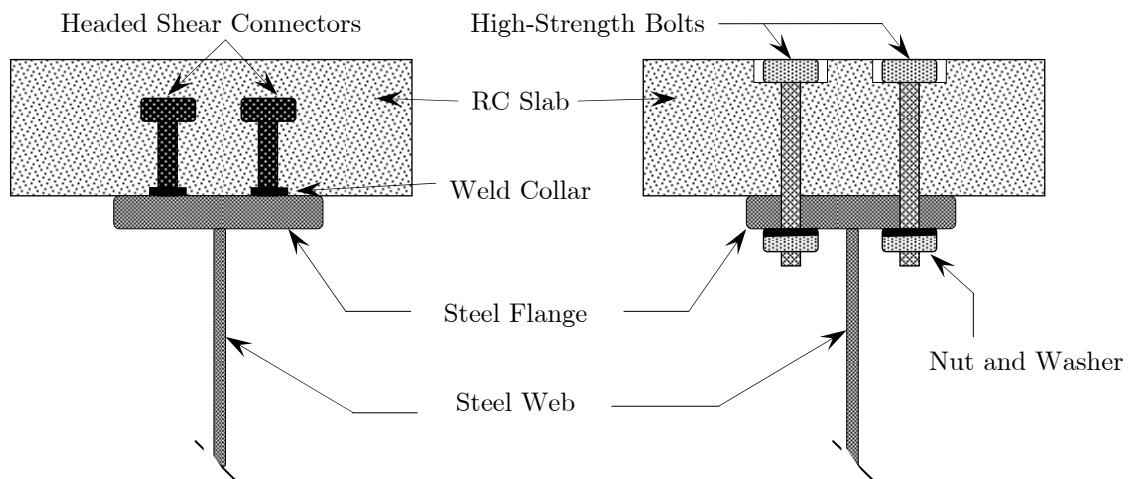


Figure 1: Headed stud connectors and high-strength bolts as shear connectors in composite beams

The testing of full-scale composite beams is costly, and so numerical techniques are very attractive in lieu of full-scale tests. In response to this, the present paper describes an efficient finite element method of analysis of composite beams with structural steel joists and ordinary Portland cement concrete slabs which are joined by high strength bolted shear connectors. It incorporates material non-linearity in these three elements of the beam, drawing on empirical representations of the shear connection response that may be obtained from standard push testing. By making recourse to a comprehensive experimental investigation undertaken in the United States some forty years ago [1, 2], the numerical model is shown to agree well with test results for full-scale beams.

Since the carbon footprint of a building transcends the procedures and materials of its original construction because of full life-cycle performance which includes its deconstruction, the use of bolted shear connectors with ordinary Portland cement slabs reduces the carbon footprint of a building that would otherwise use welded headed stud connectors with ordinary Portland cement slabs for which deconstruction is problematic. The numerical technique developed in the paper provides an efficacious tool of analysis for composite beams with high-strength bolt shear connectors, and is therefore a contribution to the numerical modelling of sustainable concrete structures.

2 Geometric non-linearity

It is known [3-5] that for non-linear large-deformation analysis, an improper treatment of the relationship between the non-linear strains and the displacements may lead to rigid body movements being superimposed onto the deformations, which produces over-stiff solutions. Herein, vector analysis and differential geometry are used to derive the relationship between the axis systems in the undeformed and deformed configurations to eliminate rigid body movements from the non-linear strains. For this, the two axis systems shown in Figure 2 are used to describe the deformations of the composite member. The first set is a body-attached (material) right-handed orthogonal system, which is in the position oyz in the undeformed configuration; the axis oz is the centroidal axis of the undeformed member and oy is the minor principal axis of the cross-section. A unit vector \mathbf{p}_z in the direction of the centroidal axis oz , and a unit vector \mathbf{p}_y in the direction of the axis oy , form a right-handed orthonormal basis vector system in $oxyz$ (Figure 2). During the deformation, the centroid o displaces w, v to the position o^* , the axis oz deforms into a curve, and so the body-attached axis system moves and rotates to a new position $o^*y^*s^*$ as shown in Figure 2. In the deformed configuration, the unit vector \mathbf{q}_z along the tangent direction of the deformed centroidal axis o^*s^* , and a unit vector \mathbf{q}_y in the direction of the minor principal axis o^*y^* of the rotated cross-section, also form an orthonormal basis vector system in the axes $o^*x^*y^*s^*$. The basis vectors $\mathbf{q}_y, \mathbf{q}_z$ attach to the member and move with it during the deformation, with the vector \mathbf{q}_z remaining normal to the cross-section at all times.

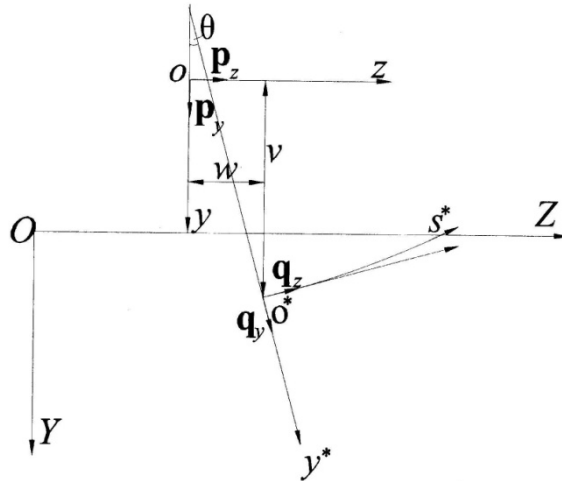


Figure 2: Axes and rotations

The second set of axes OYZ is a space-fixed (space) right-handed rectangular coordinate system, as also shown in Figure 2, with axes OY and OZ parallel to the axes oy and oz of the system oyz in the undeformed configuration. The positions of

the member in the undeformed and deformed configuration can be defined in the axis system OYZ .

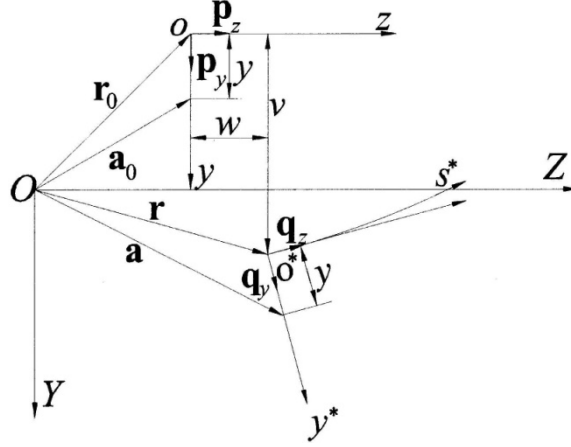


Figure 3: Position vectors

The relationship between the basis vectors ($\mathbf{q}_y, \mathbf{q}_z$) in the deformed configuration and the basis vectors ($\mathbf{p}_y, \mathbf{p}_z$) and the undeformed configuration can be expressed as

$$\mathbf{q}_y = \cos \theta \mathbf{p}_y - \sin \theta \mathbf{p}_z \quad \text{and} \quad \mathbf{q}_z = \sin \theta \mathbf{p}_y + \cos \theta \mathbf{p}_z, \quad (1)$$

where θ is the angle between the axes oy and o^*y^* (or between the axis oz and the tangent to the axis o^*s^*), as shown in Figure 2. Vector analysis can be used to express $\cos \theta$ and $\sin \theta$ in terms of the axial and radial displacements w and v . In the undeformed configuration, the position vector of the centroid o in the fixed axis system OYZ is \mathbf{r}_0 as shown in Figure 3, and so the unit vector \mathbf{p}_z at the centroid o can be expressed in terms of \mathbf{r}_0 as [3]

$$\mathbf{p}_z = d\mathbf{r}_0/dz. \quad (2)$$

In the deformed configuration, the position vector of the centroid o^* in the fixed axis system OYZ is \mathbf{r} , as shown in Figure 3, and so the vector \mathbf{q}_z can be obtained by differentiating the position vector \mathbf{r} of the centroid o^* with respect to the arc length s^* of the axis o^*s^* as

$$\mathbf{q}_z = \frac{d\mathbf{r}}{ds^*} = \left(\frac{1}{1 + \varepsilon} \right) \frac{d\mathbf{r}}{dz}, \quad (3)$$

where $ds^* = (1 + \varepsilon)dz$ is used, with ε being the longitudinal normal strain at the centroid defined by

$$1 + \varepsilon = \sqrt{(1 + w')^2 + v'^2}, \quad (4)$$

and where primes denote differentiation with respect to z . In the deformed configuration, the position vector \mathbf{r} can be expressed as (Figure 3)

$$\mathbf{r} = \mathbf{r}_0 + v\mathbf{p}_y + w\mathbf{p}_z, \quad (5)$$

and substituting Equations (2) and (5) into (3) leads to

$$\mathbf{q}_z = \left(\frac{1}{1 + \varepsilon} \right) \left[v'\mathbf{p}_y + (1 + w')\mathbf{p}_z \right] = \hat{v}'\mathbf{p}_y + \hat{w}'\mathbf{p}_z, \quad (6)$$

in which $\hat{v}' = v'/(1 + \varepsilon)$ and $\hat{w}' = (1 + w')/(1 + \varepsilon)$. A comparison of Equations (1) and (6) then gives accurate values for $\cos\theta$ and $\sin\theta$ as

$$\cos\theta = \hat{w}' \quad \text{and} \quad \sin\theta = \hat{v}'. \quad (7)$$

In the $o^*y^*s^*$ system, the Frenet-Serret formulae of differential geometry define the relationship between the curvature κ and the unit vectors \mathbf{q}_y and \mathbf{q}_z in the deformed configuration as

$$d\mathbf{q}_y/ds^* = \kappa\mathbf{q}_z \quad \text{and} \quad d\mathbf{q}_z/ds^* = -\kappa\mathbf{q}_y, \quad (8)$$

from which the curvature κ in the deformed configuration can be obtained as

$$\kappa = \frac{1}{(1 + \varepsilon)} \frac{d\mathbf{q}_y}{dz} \cdot \mathbf{q}_z \quad \text{or} \quad \kappa = -\frac{1}{(1 + \varepsilon)} \frac{d\mathbf{q}_z}{dz} \cdot \mathbf{q}_y. \quad (9)$$

Substituting Equations (1) and (7) into either of Equations (9) then leads to the expression for the curvature in the deformed configuration as

$$\kappa = \frac{1}{(1 + \varepsilon)} \left(\hat{v}''\mathbf{p}_y + \hat{w}''\mathbf{p}_z \right) \left(\hat{w}'\mathbf{p}_y - \hat{v}'\mathbf{p}_z \right) = \frac{\hat{v}'\hat{w}'' - \hat{w}'\hat{v}''}{1 + \varepsilon}, \quad (10)$$

or

$$\kappa = \frac{v'w'' - v''(1 + w')}{\left[(1 + w')^2 + v'^2 \right]^{3/2}} \quad (11)$$

and which can be simplified further to the familiar expression for the curvature as

$$\kappa = \frac{-v''}{\left[1 + v'^2 \right]^{3/2}} \quad (12)$$

if the effect of the axial extension w' is ignored.

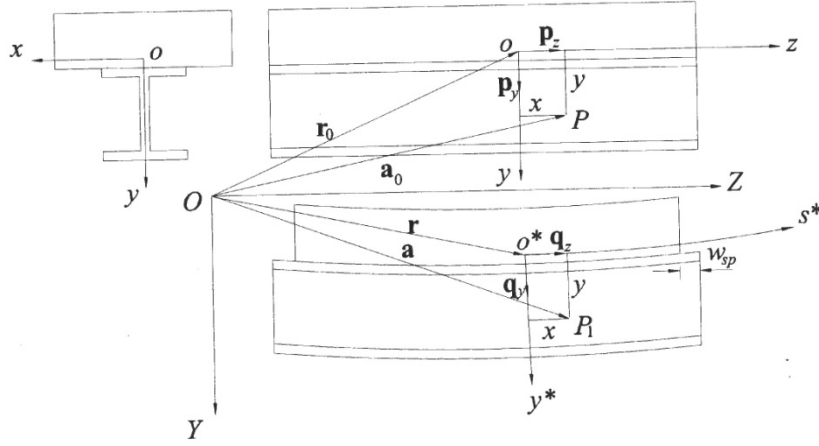


Figure 4: Interface slip and deformations

In order to include interface slip in the non-linear formulation, the total deformation of a material point P on the cross-section of the member is considered to result from two successive motions: a translation and finite rotation of the cross-section, and a superimposed relative slip displacement between the steel joist and concrete slab along the unit vector \mathbf{q}_z shown in Figure 4. Because the slip displacement $w_{sp}(z)$ is a relative axial displacement between the steel and concrete, its sign is opposite for the steel joist and concrete slab. Under these two assumptions, the position vector \mathbf{a} and the deformation gradient tensor \mathbf{F} of the material point after the deformation can be expressed as (Figure 4)

$$\mathbf{a} = \mathbf{r} + y\mathbf{q}_y \mp w_{sp}(z)\mathbf{q}_z \quad \text{and} \quad \mathbf{F} = \left\{ \frac{\partial \mathbf{a}}{\partial y}, \frac{\partial \mathbf{a}}{\partial z} \right\} = \left\{ \frac{\partial \mathbf{a}}{\partial y}, (1 + \varepsilon) \frac{\partial \mathbf{a}}{\partial s} \right\}, \quad (13)$$

in which the sign of the term $w_{sp}(z)\mathbf{q}_z$ is negative (-) for a material point in the slab and positive (+) for a material point in the steel joist.

The strain tensor is

$$\begin{bmatrix} \varepsilon_{yy} & \frac{1}{2}\gamma_{yz} \\ \frac{1}{2}\gamma_{zy} & \varepsilon_{zz} \end{bmatrix} = \frac{1}{2}(\mathbf{F}^T\mathbf{F} - \mathbf{I}), \quad (14)$$

from which the normal strains are given as

$$\varepsilon_{yy} = 0; \varepsilon_{zz} \approx w' \mp w'_{sp} + \frac{1}{2}v'^2 + \frac{1}{2}w'^2 + \frac{1}{2}w'_{sp}{}^2 - y[v''(1+w') - v'w''] \pm yv''w'_{sp}, \quad (15)$$

and the shear strains are given as

$$\gamma_{zy} = \gamma_{yz} = \mp v''w'_{sp}, \quad (16)$$

which are induced by the interaction between the slip and the in-plane bending. If geometric non-linearity were not considered, these shear strains in the steel and concrete slab would vanish.

3 Material non-linearities

The material models for steel and concrete have been presented and discussed elsewhere [3], and so a brief summary only is presented here. For the steel joist in compression and tension, the von Mises yield criterion can be written in terms of the stress vector $\boldsymbol{\sigma}$ as

$$F(\boldsymbol{\sigma}, \lambda) = \sigma_e - \sigma_y = 0, \quad (17)$$

in which σ_y is the uniaxial yield stress determined from a suitable hardening parameter H'_s and $\sigma_e = \sqrt{(\sigma_{zz}^2 + 3\tau_{zy}^2)}$ is the effective stress. Based on the associated flow and isotropic hardening theory, the relationship between the stress and total (elastic and plastic) strain increments is

$$d\boldsymbol{\sigma} = \mathbf{E}^{ep} d\boldsymbol{\varepsilon}, \quad (18)$$

where \mathbf{E}^{ep} is the standard tangent modulus material matrix [3].

For concrete in tension, the concrete is assumed to be elastic with a crack detection surface being represented as

$$F_t(\boldsymbol{\sigma}, \lambda_t) = \sigma_e^t - \left[3 - b_0 \left(\sigma_t / \sigma_t^u \right) \right] p^t - \left[2 - (b_0/3) \left(\sigma_t / \sigma_t^u \right) \right] \sigma^t = 0, \quad (19)$$

where σ_e^t is the von Mises equivalent deviatoric stress (the same as for the steel), p^t the effective tensile stress, $\sigma_t(\lambda_t)$ the hardening parameter, σ_t^u the ultimate stress in uniaxial tension and b_0 a constant [6]. After cracking, tensile stresses are generated in the cracked slab as a result of transfer, via shear and bond, of the stresses from the reinforcement and the steel component. The constitutive model therefore includes tension stiffening [7], which is incorporated into the tangent material matrix \mathbf{E}^{cr} in $d\boldsymbol{\sigma} = \mathbf{E}^{cr}d\boldsymbol{\varepsilon}$.

For concrete in compression, the compression yield surface is represented by

$$F_c(\boldsymbol{\sigma}, \lambda) = \sigma_e^c - \sqrt{3}a_0p^c - \left(1 - a_0/\sqrt{3}\right)\sigma_c = 0, \quad (20)$$

where $p^c = -\sigma_{zz}/2$, σ_e^c is the von Mises equivalent deviatoric stress (the same as for the steel), $\sigma_c(\lambda)$ the hardening parameter and a_0 a constant [6]. The associated flow rule generally over-predicts the inelastic volume strain. However, for computational efficiency and simplicity in the line element, the associated flow and isotropic hardening rules are also used for the concrete component when compression is dominant.

To account for the non-linear shear force and slip relationship using a high strength bolted shear connection, the FE model provides the facility for the incremental relationship between the slip w_{sp} and the shear force Q_{int} at the interface. To input the correct incremental relationship between the slip and shear force, the empirical non-linear shear force versus slip characteristics at the interface can be obtained from push tests [8].

Parameterisation of empirical push tests has been reported in research outcomes, and the non-linear model proposed by Yam and Chapman [9] is widely-accepted for headed stud connectors in composite beams. They proposed that

$$Q_{int} = a \left[1 - \exp(-bw_{sp}) \right], \quad (21)$$

where a and b are constants that can be obtained from two points on the experimental curve as

$$a_1 = \frac{Q_1^2}{2Q_1 - Q_2} \quad \text{and} \quad b = \frac{1}{w_{sp1}} \ln \left(\frac{Q_1}{Q_2 - Q_1} \right). \quad (22)$$

Very little research has been published using high-strength bolts as shear connectors. Dallam [1] undertook 12 push tests using high strength bolts, and a typical empirical curve using Equation (21) is compared with Dallam's results in Figure 5. For larger slips, the empirical representation of Equation (21) and the push tests for high-strength bolted shear connectors does not agree well, and so an alternate representation based on the results of Dallam [1] is proposed here as

$$w_{sp} = \frac{Q_{int}}{K_l} + \frac{p}{10} \left(\frac{Q_{int}}{Q_n} \right)^c, \quad (23)$$

where K_l is the linear shear stiffness at the interface obtained from push tests, Q_n the shear force at which the relationship between the slip displacement and shear force at the interface becomes non-linear (as obtained from tests) and the parameters p and c are chosen to match the experimental data. In Figure 5, using $p = 10$ and $c = 10$ results in good correlation with the tests of Dallam [1].

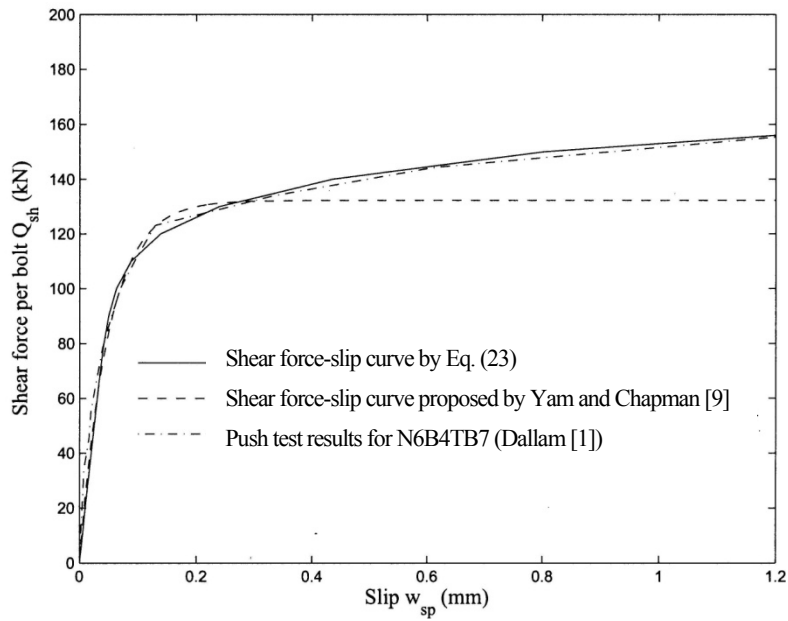


Figure 5: Non-linear relationship between shear force and slip at interface

The tangent relationship between the slip increment and shear force increment in Equation (23) is

$$dw_{sp} = \frac{dQ_{int}}{K_l} + \left(\frac{cpQ_{int}^{c-1}}{10Q_n^c} \right) dQ_{int}. \quad (24)$$

To facilitate the slip displacement in the element, it is assumed that the shear connection between the slab and steel joist acts as a continuous medium along the length of the element, and that the shear connectors are distributed uniformly along the length of a composite member. Hence,

$$q_{int} = Q_{int}/s_{sh} \quad (25)$$

where s_{sh} is the spacing between adjacent bolt connectors. Finally, the incremental slip can be obtained in the tangent stiffness formation

$$dq_{int} = K_{int} dw_{sp}, \quad (26)$$

where

$$K_{int} = \frac{10K_l Q_n^a}{s(10Q_n^a + apK_l Q_{int}^{a-1})} \quad (27)$$

is the tangent stiffness of the high-strength bolted shear connection.

4 Non-linear equilibrium

The non-linear equations of equilibrium for a beam element can be derived from the principle of virtual displacements, which requires that

$$\int_{vol} \delta \boldsymbol{\varepsilon}^T \boldsymbol{\sigma} d(vol) + \int_{\ell} \delta w_{sp} q_{sh} dz - \int_{\ell} \delta \mathbf{u}^T \mathbf{q} dz - \sum_k \delta \mathbf{u}_k^T \mathbf{Q}_k = 0 \quad (28)$$

for all kinematically admissible virtual displacements δv , δw , δw_{sp} , and where $\boldsymbol{\sigma} = \{\sigma_{zz}, \tau_{zy}\}^T$, $\delta \boldsymbol{\varepsilon} = \{\delta \varepsilon_{zz}, \delta \gamma_{zy}\}^T$, q_{sh} and δw_{sp} are the shear flow force and conjugate virtual slip at the slab-joist interface, \mathbf{q} , \mathbf{Q}_k and $\delta \mathbf{u}$ are vectors of the external distributed and concentrated loads and the vector of conjugate virtual displacements. The efficient method herein is reliant on the principle of consistent linearization of the principle of virtual displacements, which plays a key role in the numerical implementation employing an incremental-iterative solution procedure. The full description of the technique in a generic framework for composite beams has been described by Pi *et al.* [3], and it is able to produce efficacious solutions for composite members.

5 Applications

As noted previously, studies of beams with bolted shear connectors do not appear to have been reported to any extent in the published literature, except for the results of Dallam and Harpster [1, 2] which are used herein to validate the results of the FE procedure. The tests were carried out on six full-scale simply supported composite beams using high-strength bolts as shear connectors. The bolts were placed through pre-drilled holes in the top flange of the steel beam and were tensioned after the

concrete had cured. The six full-scale composite beams were tested in two series and each series consists of three beams. The dimensions, the cross-section and the loadings of the first and second series are shown in Figures 6 and 7 respectively.

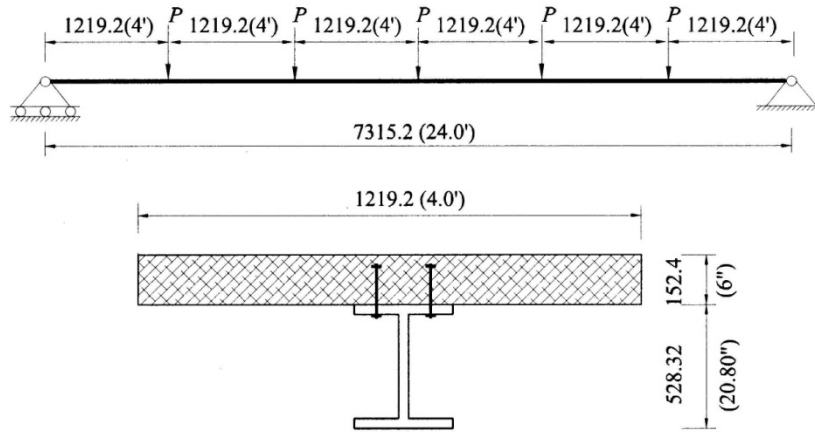


Figure 6: Bolted composite beam (first series)

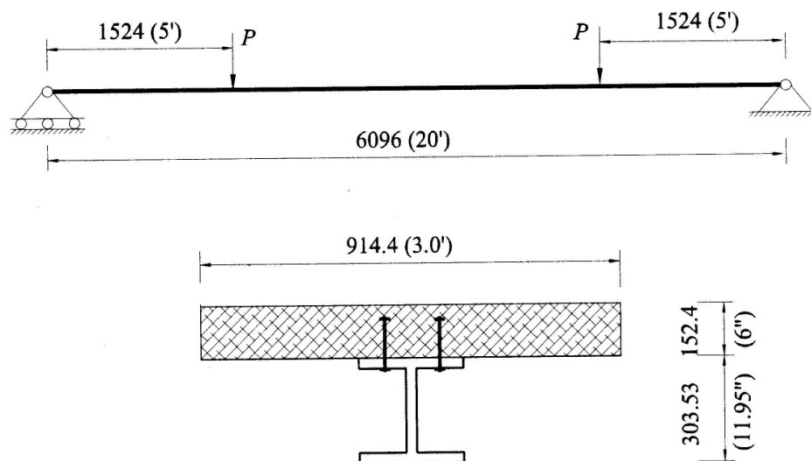


Figure 7: Bolted composite beam (second series)

The FE results for the variations of the central deflection v_c with the load per jack P are compared with the test results of Dallam and Harpster [2] in Figure 8 for beams NFB6B2 of the first series, and in Figure 9 for beams NFB4B2 of the second series. Eight beam elements were used to model the composite beams. Tables 1 and 2 give the material properties for the steel and concrete respectively, while for the FE computations, the shear force-slip relationships given by Equation (26) with the appropriate parameters from the push tests [1] were used. For beam NFB6B2, the non-linear behaviour starts at a load $P = 140$ kN. As the load increases, yielding increases at mid-span and spreads to other sections of the beam and when it reaches

$P = 205$ kN, the composite beam with high-strength bolted shear connectors fails by crushing of the concrete slab at the mid-span of the beam. The behaviour for beam NFB4B2 is very similar, with non-linearity commencing at $P = 150$ kN and crushing when the load reaches $P = 210$ kN. Importantly, the agreement between the computational model and the test results is very good.

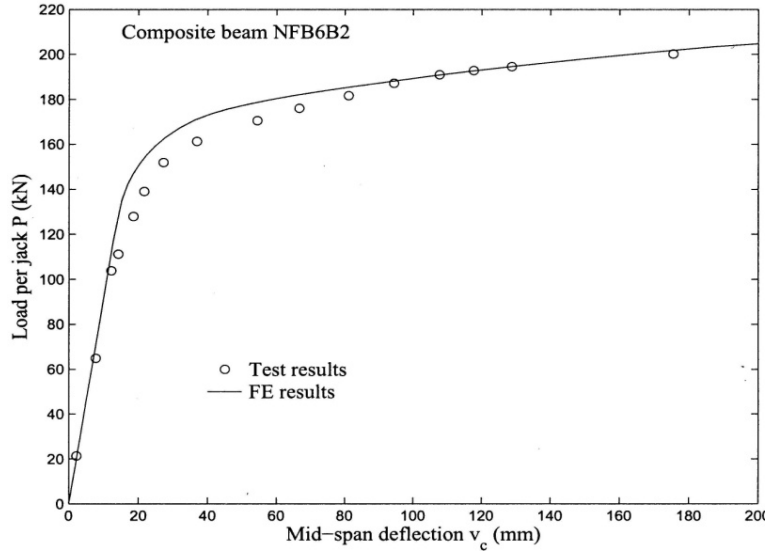


Figure 8: Comparisons of computational and experimental transverse deflections (NFB6B2)

The FE results for the end slips are also compared with the test results as the variations of the end slip with the load per jack in Figure 10 for beam NFB6B2 and in Figure 11 for beam NFB4B2. Again, it can be seen that the agreement between the numerical and test results is very good.

Specimen	Elastic Modulus E_s		Yield Strength σ_s			
			Web		Flange	
	psi $\times 10^6$	kN/mm ²	psi $\times 10^3$	N/mm ²	psi $\times 10^3$	N/mm ²
NFB4B2	29.0	200	38.0	262	36.6	252
NFB6B2	29.1	201	38.2	263	37.2	256

Table 1: Steel material properties used in numerical model

Specimen	Elastic Modulus E_c		Compressive Strength σ_c		Unit Weight	
	psi $\times 10^6$	kN/mm ²	psi $\times 10^3$	N/mm ²	pcf	kg/m ³
NFB4B2	4.19	28.9	6.89	47.5	137.5	2195
NFB6B2	4.57	31.5	7.13	49.2	144.0	2307

Table 2: Concrete material properties used in numerical model

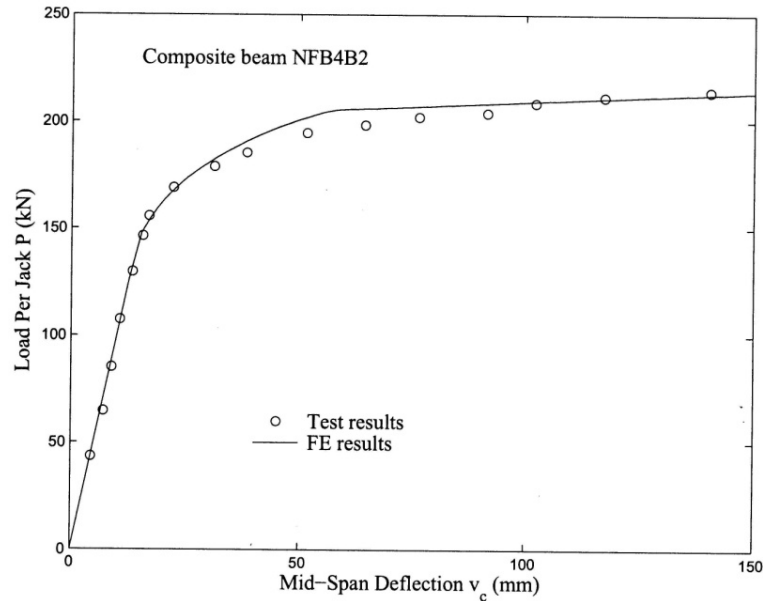


Figure 9: Comparisons of computational and experimental transverse deflections (NFB4B2)

6 Concluding remarks

This paper has presented a non-linear finite element model for analysing the response of composite steel-concrete beams for use in deconstructable framed buildings. The focus has been on incorporating a variety of material non-linearities, and in particular, the technique is applicable to representing the shear connection between the joist and slab using high-strength bolts. The test results reported elsewhere elucidate the significant ductility that accrues to the use of high-strength bolts in lieu of conventional headed stud shear connectors welded to the flange of the steel joist. The numerical scheme is able to capture this response accurately, and so has the potential to formulate design guidelines without the need for comprehensive and costly experimental programmes.

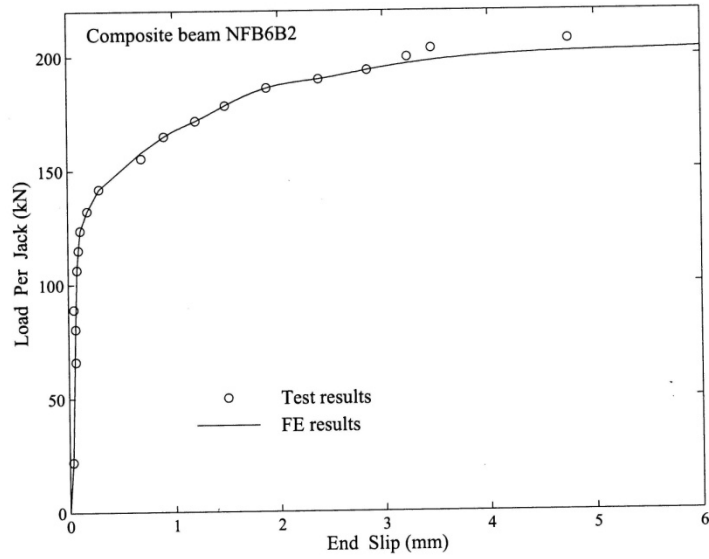


Figure 10: Comparisons of computational and experimental slip deflections (NFB6B2)

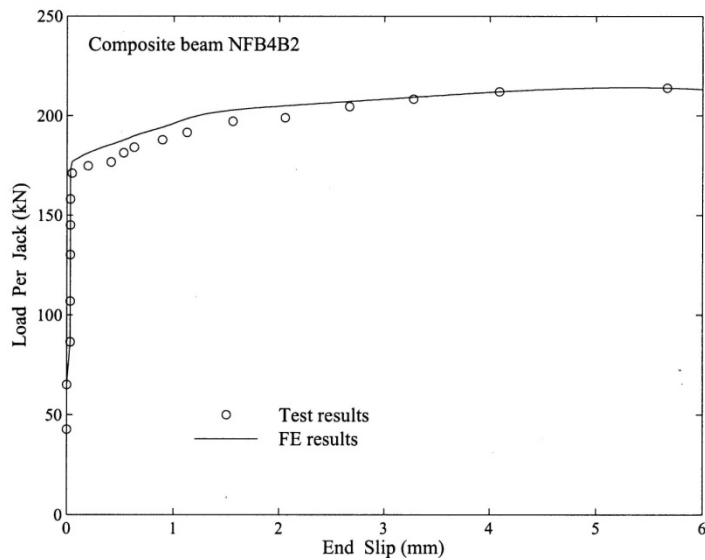


Figure 11: Comparisons of computational and experimental slip deflections (NFB4B2)

Acknowledgements

The work reported in this paper was supported by the Australian Research Council, through an Australian Laureate Fellowship (FL100100063) awarded to the first author, as well as Discovery Projects DP1097096 and DP1096454 awarded to both authors. Emeritus Professor R.P. Johnson of the School of Engineering, University of Warwick, kindly provided details of the experimental work cited in the paper.

References

- [1] L.N. Dallam, “Pushout tests with high strength bolt shear connectors”, Report 68-7, Department of Civil Engineering, University of Missouri Columbia, USA, 1968.
- [2] L.N. Dallam, J.L. Harpster, “Composite beam tests with high-strength bolt shear connectors”, Report 68-3, Department of Civil Engineering, University of Missouri Columbia, USA, 1968.
- [3] Y.-L. Pi, M.A. Bradford, B. Uy, “Second order nonlinear inelastic analysis of composite steel-concrete members. I: Theory”, *Journal of Structural Engineering*, ASCE, 132(5), 751-761, 2006.
- [4] Y.-L. Pi, M.A. Bradford, B. Uy, “A rational elasto-plastic spatially-curved thin-walled beam element”, *International Journal for Numerical Methods in Engineering*, 70(3), 253-290, 2007.
- [5] Y.-L. Pi, M.A. Bradford, F. Tin-Loi, R.I. Gilbert, “Geometric and material nonlinear analysis of elastically restrained arches”, *Engineering Structures*, 29(3), 283-295, 2007.
- [6] P. Menetrey, K.J. Willam, “Triaxial failure criterion for concrete and its generalization”, *ACI Structural Journal*, 92, 311-318, 1995.
- [7] R.I. Gilbert, R.F. Warner, “Tension stiffening in reinforced concrete slabs”, *Journal of the Structural Division*, ASCE, 104, 1885-1900, 1978.
- [8] D.J. Oehlers, M.A. Bradford, “Steel and Concrete Composite Structural Members: Fundamental Behaviour”, Pergamon Press, Oxford, UK, 1995.
- [9] L.C.P. Yam, J.C. Chapman, “The inelastic behaviour of simply supported composite beams of steel and concrete”, *Proceedings of the Institution of Civil Engineers*, London, Part B, 41(2), 651-683, 1968.